Numerical investigations of potential systematic uncertainties in iron opacity measurements at solar interior temperatures

T. Nagayama, J. E. Bailey, G. P. Loisel, G. A. Rochau, J. J. MacFarlane, and I. E. Golovkin

Phys. Rev. E **95**, 063206 — Published 26 June 2017

DOI: 10.1103/PhysRevE.95.063206

Numerical investigations of potential systematic uncertainties in iron opacity measurements at solar interior temperatures

T. Nagayama, J. E. Bailey, G. P. Loisel, and G. A. Rochau
Sandia National Laboratories, Albuquerque, New Mexico 87185, USA

J. J. MacFarlane and I. E. Golovkin
Prism Computational Sciences, Madison, Wisconsin 53711, USA
(Dated: May 18, 2017)

Iron opacity calculations presently disagree with measurements at ∼180–195 eV electron temperature and (2–4)×10^{22} cm^{-3} electron density, conditions similar to the base of the solar convection zone. The measurements use x-rays to volumetrically heat a thin iron sample that is tamped with low-Z materials. The opacity is inferred from spectrally resolved x-ray transmission measurements. Plasma self emission, tamper attenuation, temporal and spatial gradients can all potentially cause systematic errors in the measured opacity spectra. In this article we quantitatively evaluate these potential errors with numerical investigations. The analysis exploits computer simulations that were previously found to reproduce the experimentally measured plasma conditions. The simulations, combined with a spectral synthesis model, enable evaluations of individual and combined potential errors in order to estimate their potential effects on the opacity measurement. The results show that the errors considered here do not account for the previously observed model-data discrepancies.

I. INTRODUCTION

Opacity is the measure of photon absorption in matter and is a critical material property to understand energy transport in plasma via radiation. Opacity calculations for high-energy-density plasmas employ untested approximations. The lack of benchmark experiments leads to uncertainty in our understanding of plasma evolution. For example, solar evolution models do not accurately predict the location of the boundary between the solar convective zone and the radiative zone [1]. One hypothesis is an underestimate in the calculated opacities used in the solar models [1, 2]—in particular, Fe opacity [3].

Recent opacity experiments revealed severe discrepancies between modeled and measured Fe opacity at solar interior conditions [4]. At Sandia National Laboratories (SNL), a cylindrically imploding plasma called the *z-pinch dynamic hohlraum* (ZPDH) [5] volumetrically heats a *half-moon target*, which consists of a thin semicircular FeMg *sample* sandwiched by circular Be and/or CH materials, called *tampers* [Fig. 1(a)]. The implosion stagnates on the z axis, provides bright backlight radiation, and permits measurements of FeMg-attenuated (I_ν) and –unattenuated (I_0) spectra on x-ray film [Fig.1(b)]. The sample transmission, T_ν, and opacity, κ_ν, are both functions of photon frequency ν and related to the measured spectra by the following equation:

$$T_\nu = \frac{I_\nu}{I_0} = e^{-\kappa_\nu \rho L}, \tag{1}$$

where ρL (g/cm^2) is the areal density of the sample, measured prior to the experiments. The sample temperature and density are inferred from the measured Mg K-shell spectra [6]. Fe opacities are calculated at the inferred conditions and compared against the measured opacities to benchmark the calculation [4].

Fig. 1(c) shows the discrepancies observed in the modeled-measured Fe opacity at 182 eV in electron temperature (T_e) and at 3×10^{22} cm^{-3} in electron density (n_e) from Ref. [4]. The measured opacity was generally higher than predictions. There are three different types of disagreement. At wavelength $\lambda < 9.5$ Å, predicted opacity is dominated by bound-free (b-f) absorption, which was systematically lower in the calculation. The calculated opacity showed significantly narrower and stronger bound-bound (b-b) line absorption features above 10 Å. Around 11.2 and 12 Å, the calculation shows opacity valleys called *windows*. These windows are important in modeling plasma evolution because radiation energy is effectively transferred through these low-opacity windows. However, such window did not exist in the measured opacity. While the discrepancy explained about half of the opacity revision needed to resolve the solar problem, the challenging nature of the experiments and the broad impact of the results suggest the experimental methods deserve continued scrutiny.

There are experimental concerns such as plasma self-emission, tamper-transmission difference (defined below), and time- and space-gradient effects. It is not straightforward to quantify exactly how these concerns would affect the opacity measurements. If plasma self-emission is important, correcting for it would raise the inferred opacity. Thus, this potential error could partially explain the disagreement in the b-b but make the b-f disagreement even worse. If the tampers are heated differently with and without the FeMg sample, the tamper transmission would not cancel exactly; it would raise the measured sample opacity. If this error is important, it may explain the disagreement in the b-f and windows, but the disagreement in the b-b would be worse. The time- and space-integration effects would affect the measured opacity in a complex way.

To zeroth order, these issues were confirmed to be neg-

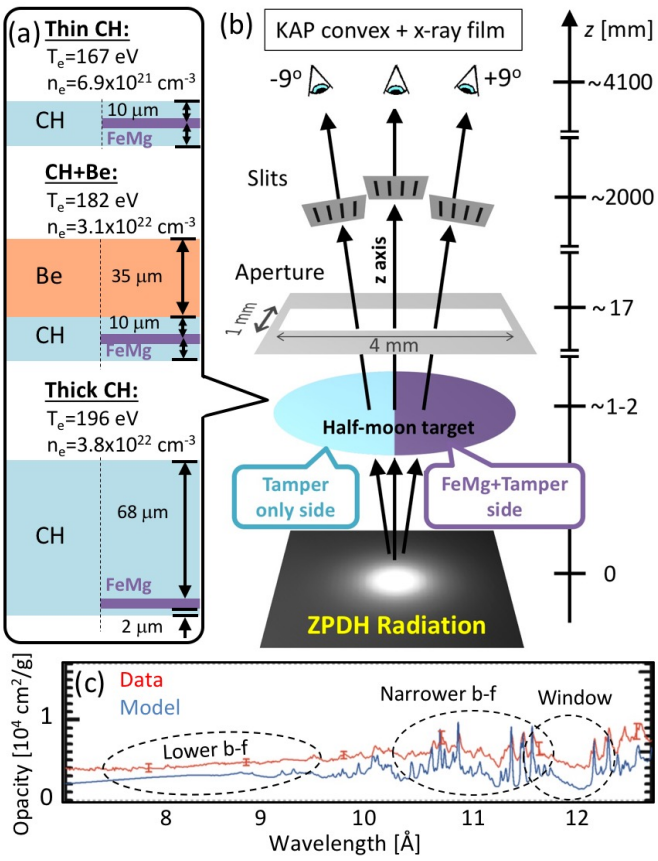

FIG. 1. (Color online) (a) Cross sections of the different target configurations, their labels, and the typical conditions. The tamper mass above the sample controls the sample conditions. (b) Experimental setup: Z opacity science platform measures FeMg-attenuated and -unattenuated spectra in a single shot experiment due to the finite backlight-to-sample distance, half-moon sample, and spectrometers fielded along ±9°. (c) Comparison of measured and modeled Fe opacity at T_e = 182 eV and $n_e = 3.1 \times 10^{22}\,\mathrm{cm}^{-3}$ from Ref. [4]. The lower curve (blue) is the calculated opacity [7], which shows lower bound-free opacity, narrower bound-bound lines, and distinct opacity windows than the measured opacity (red, upper). We confirmed similar discrepancies from all models compared in [4].

ligible [3, 4, 6]. However, this interpretation was done in a *static-uniform-plasma* picture, and full evaluation requires consideration of time- and space-dependent effects.

In this paper, we use the simulation developed in Ref. [8] and quantify the potential systematic errors in the experiment that augment the error analysis provided in Ref. [4]. We infer the ZPDH radiation drive using measured gated pinhole images and three-dimensional (3-D) view-factor model VISRAD [9]. The sample plasma evolution was simulated with the 1-D hydrodynamic simulation model HELIOS [10, 11]. The modeled sample plasma and ZPDH radiation were post-processed to simulate the spectral image measurements. The conditions inferred from Mg lines of the synthetic data agree with those from the experiments [8]. The simulation performed without the FeMg sample successfully reproduced the measured backlight spectral images, showing agreement in spectral and spatial shapes and in brightness. While the potential systematic uncertainties are complicated and intertwined, the simulation permits us to turn on and off each source of systematic error to isolate and investigate one issue at a time.

We find that the plasma self-emission can lower the opacity by 40% at wavelengths greater than 12.7 Å but is negligible over the spectral range reported by Bailey *et al* [4]. The tamper transmission difference could artificially raise the measured opacity by a few percent but is too small to explain the reported discrepancy. Finally, we investigate the impact of the temporal and spatial gradients. While the simulated temporal gradients in T_e and n_e were 14% and 70%, respectively, and notable, the synthetic experimental spectra successfully represent Fe opacity at the single T_e and n_e inferred from the Mg spectra. The simulated gradients do not introduce significant error in the opacity measurements. Overall, the potential sources of systematic uncertainty investigated here are found to be negligible and do not explain the discrepancies reported by Bailey *et al* [4].

The rest of the article is organized as follows. Sec. II discusses criteria for reliable opacity measurements, the Z opacity measurement platform, and assumptions in the data analysis. Sec. III summarizes potential systematic uncertainties in our opacity measurements due to the assumptions. Sec. IV discusses the synthetic investigations and their results. Sec. IV A provides simulation details. Sec. IV B shows the overall effects of plasma self-emission, tamper-transmission differences, and time- and space-integration. Sec. IV C, IV D, and IV E break down the impact of each effect. The conclusion is given in Sec. V.

II. Z OPACITY MEASUREMENTS AND CRITERIA FOR RELIABILITY

Figure 1(b) illustrates the SNL Z opacity experimental setup. The *half-moon* target consists of a semi-circular FeMg *sample* sandwiched by a circular *tamper* (e.g., CH and Be). The half-moon target is placed above the *z-pinch dynamic hohlraum* (ZPDH) radiation source. The target is radiatively heated as the ZPDH plasma implodes and is backlit at stagnation [3, 5, 8]. The sample temperature and density are controlled by the tamper configuration [6]. Figure 1(c) shows the three tamper configurations and the achieved conditions measured with Mg K-shell spectroscopy. The sample-transmitted backlight radiation is measured by potassium acid phthalate (KAP) crystal spectrometers fielded along ±9° with respect to the z axis [12, 13]. Slits provide spatial resolution across the half-moon boundary. Taking advantage of the finite source-to-sample distance, the half-moon target, and the ±9° spectrometer alignment, this

platform measures the sample-attenuated (at +9°) and -unattenuated (at -9°) spectra in a single experiment. The data are recorded on x-ray film.

We can approximate FeMg transmission by $I_\nu^{+9^\circ}/I_\nu^{-9^\circ}$ as in Eq. (1). We can extract the sample (i.e., FeMg) opacity by converting the measured transmission to opacity using the areal density inferred with Rutherford backscattering techniques, which were performed prior to the experiments. However, this transmission is not exactly equal to the FeMg transmission because of the finite spectral resolution of the instrument, plasma self-emission, and the slight tamper attenuation difference on the two sides of the half-moon target. More accurately, the measured transmission is expressed as follows:

$$T_\nu^{\text{measured}} = \frac{\tilde{I}_\nu^{+9^\circ}}{\tilde{I}_\nu^{-9^\circ}} \tag{2}$$

with

$$\tilde{I}_\nu^{\pm 9^\circ} = \int I_{\nu'}^{\pm 9^\circ} g_{\nu-\nu'} d\nu', \tag{3}$$

where $g_{\nu-\nu'}$ is a convolution function for the instrumental broadening. $I_\nu^{\pm 9^\circ}$ consists of the transmitted backlight radiation and the emergent plasma self-emission:

$$\begin{aligned} I_\nu^{+9^\circ} &= BT_aT_{\text{FeMg}}T_b \\ &\quad + I_aT_{\text{FeMg}}T_b + I_{\text{FeMg}}T_b + I_b \end{aligned} \tag{4}$$

$$I_\nu^{-9^\circ} = BT_c + I_c \tag{5}$$

where their notations are explained in Fig. 2. The four terms in Eq. (4) are the backlight radiation transmitted through the sample and the tamper, bottom tamper self-emission transmitted through the sample and the top tamper, FeMg sample self-emission transmitted through the top tamper, and the top tamper self-emission, respectively. The two terms in Eq. (5) are the backlight radiation transmitted through the tamper and the emergent tamper self-emission. Here, the subscript ν that indicates the frequency dependence is omitted from the right-hand side for simplicity, but all quantities are frequency dependent. We also neglect the space- and time-dependence within each component at the moment, which are taken into account in detail in the later section. This refined picture of our measurement clarifies some of the important requirements for accurate T_{FeMg} measurements.

First, one has to minimize the impact of self-emission. This requires either a very accurate simultaneous measurement of frequency-resolved self-emission or a very bright backlight so that backlight radiation attenuated through the target is much brighter than the emerging self-emission:

$$BT_aT_{\text{FeMg}}T_b \gg I_aT_{\text{FeMg}}T_b,\ I_{\text{FeMg}}T_b, \text{ and } I_b \tag{6}$$

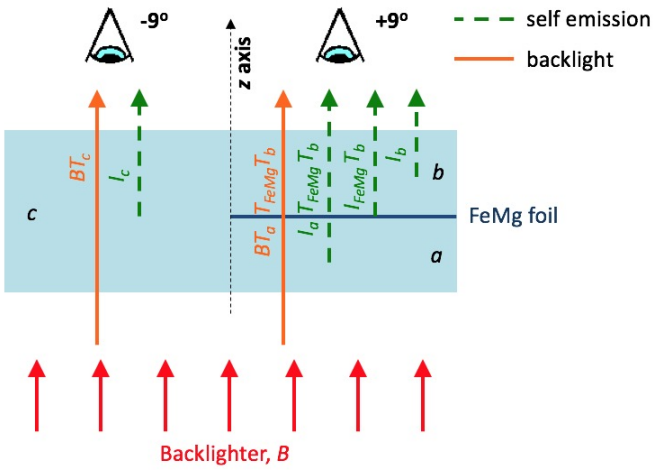

FIG. 2. (Color online) Signal detected by the spectrometer at ±9°. Backlight (red) is attenuated by tamper at −9° and by FeMg foil and tamper at +9° (orange). Self-emission (green) is attenuated by all plasmas between the emission source and the detector. B indicates backlight radiation, and T_X is transmission of component X where $X = a$, b, c, and FeMg. Components a and b are the bottom and top tampers on the FeMg-embedded side, respectively. Component c is the tamper on the tamper-only side. I_X is the emergent self-emission at component X where the self-absorption within the component is taken into account.

$$BT_c \gg I_c. \tag{7}$$

If the impact of the self-emission is minimized, the measured transmission can be written as:

$$T_\nu^{\text{measured}} \approx \frac{\int (BT_aT_{\text{FeMg}}T_b)_{\nu'}\, g_{\nu-\nu'} d\nu'}{\int (BT_c)_{\nu'}\, g_{\nu-\nu'} d\nu'}. \tag{8}$$

where $()_{\nu'}$ simply means that every quantity inside the parenthesis is a function of frequency ν'. The tamper material consists of low atomic-number elements so that the tamper transmission (or emission) do not produce any spectral line features in the x-ray range of interest. Thus, with good spectral resolution, the change in continuum backlight radiation and tamper transmission over the $g_{\nu-\nu'}$ width becomes negligible. Then, by moving those continuum terms outside the integral, we can write:

$$\begin{aligned} T_\nu^{\text{measured}} &\approx \frac{(BT_aT_b)_\nu \int T_{\nu',\,\text{FeMg}} g_{\nu-\nu'} d\nu'}{(BT_c)_\nu \int g_{\nu-\nu'} d\nu'} \\ &\approx \left(\frac{T_aT_b}{T_c}\right)_\nu \int T_{\text{FeMg}} g_{\nu-\nu'} d\nu', \end{aligned} \tag{9}$$

which clarifies another requirement:

$$T_aT_b \approx T_c \tag{10}$$

at every frequency, ν, of our interest. This can be achieved either by using an optically thin tamper so that $T_a \approx T_b \approx T_c \approx 1$ or using volumetric heating to achieve similar axial-condition profiles in the tampers at both the

FeMg-embedded side (i.e., T_aT_b side) and tamper-only side (i.e., T_c side).

To summarize, accurate transmission measurements require:

R1: Spectra have to be accurately measured

R2: Instrumental spectral resolution has to be sufficiently high to resolve key line features and measured accurately prior to the experiments

R3: Backlight radiation and tamper transmission have to be free of wavelength-dependent structure [Eq. (9)]

R4: Plasma self-emission has to be minimized [e.g., Eqs. (6) and (7)]

R5: Tamper transmission difference has to be minimized [i.e., Eq. (10)]

Once these criteria are met, measured transmission spectra can be compared with modeled transmission after convolving it with the instrumental broadening function $g_{\nu-\nu'}$ [Eq. (3)]. In order to test Fe opacity for the convection-zone-base (CZB) problem, there are a few more criteria:

R6: Sample is heated to the conditions relevant to CZB

R7: Sample condition is uniform, achieving near local thermodynamic equilibrium (LTE)

R8: Sample temperature, density, and drive radiation are independently measured

R9: Measurements are repeated with multiple sample thicknesses to ensure accurate opacity measurements over wide dynamic range

The last requirement needs further explanation. Opacity measurement is more reliable if its transmission is measured between 0.2-0.8. As the transmission approaches unity, the precision of the opacity measurement deteriorates because the measured absorption (i.e., 1-T) becomes smaller than the measurement uncertainty. As the transmission approaches zero, the accuracy of the measurement degrade because it becomes more susceptible to the inaccuracy of the background subtraction. Thus, measuring opacity with different sample thickness is critical to test the measurement accuracy and necessary for accurate and precise opacity measurements over wide dynamic range.

To zeroth order, the Z opacity science platform satisfies these criteria [3, 6, 13]. The spectra were accurately measured by KAP spectrometers that provided a resolving power greater than 900 [14]. The instrumental broadening profile was accurately measured with a Manson source [14] and applied to the modeled transmission spectra [15]. The backlight radiation was 314-eV quasi-Planckian radiation for previous experiments [13, 15] and 350-eV for newer experiments [4, 6], which are much brighter than 150-eV and 195-eV plasma self-emission, respectively. Low-opacity materials, CH or Be, were selected for the tamper, and the attenuation in the tamper was minimal. Also, since the same thickness and composition of the tampers were volumetrically heated with the ZPDH radiation, the tampers at the FeMg-embedded side and tamper-only side are expected to have similar conditions and similar transmission. Large mm-scale samples were uniformly heated to solar-interior conditions using the volumetric heating provided by the energetic ZPDH radiation [3, 6]. The sample uniformity was experimentally validated with spectroscopic measurements [6]. The sample conditions were independently characterized using Mg K-shell spectroscopy [6, 13, 15]. The potential inaccuracy of K-shell spectroscopy and its impact on the measurements were numerically investigated and found to be negligible [16]. The reliability of the measured opacities was confirmed by performing experiments with two or three different sample thicknesses at each of the three conditions achieved [Fig. 1], and their variations were added into the measurement uncertainties [4, 15].

III. POTENTIAL SYSTEMATIC UNCERTAINTIES

One concern in the validation of the Z experimental platform discussed in Sec. II is the fact that the data are interpreted in a *static-uniform plasma* picture. In reality, x-ray film records x-ray signals throughout the entire experiment duration over which the plasma continuously changes its conditions. This static-uniform picture is supported because the signal is dominated by that from the backlight radiation, which is bright only for 3 ns. Since the sample is slowly cooling at the time of the backlight radiation, the change in sample conditions over this duration is expected to be negligible [3, 13, 15]. In addition, Bailey *et al.* [15] reported excellent agreement between measured and modeled Fe opacity at $T_e = 156$ eV and $n_e = 6.9 \times 10^{21}\,\mathrm{cm}^{-3}$. The agreement supports not only the validity of the opacity models at these conditions but also the validity of the experimental platform. If the Z opacity experiments suffered from serious temporal or axial gradients, such excellent agreement would not have been achieved. Nonetheless, recent simulations [8] suggested that the sample T_e and n_e would drop by 14% and 70%, respectively, over this 3-ns backlight duration. The experimental systematic uncertainties need to be rescrutinized by taking into account this *dynamic-gradient plasma* reality in experiments to see how much the temporal integration could affect the former investigations.

For example, the importance of self-emission needs to be reinvestigated. While the temperature comparison suggests that the backlight radiation (314–350 eV) is much brighter than plasma self-emission (150–195 eV), the validity of such a comparison is limited without careful assessment of the potential difference in duration,

area, and solid angle between the self-emission and backlight radiation. If FeMg self-emission lasted longer or was emitted from a larger area than that of backlight radiation, the self-emission is not as negligible as originally investigated. One goal of the present work is to use simulations that account for emission area, duration, and solid angle of both plasma self-emission and backlight radiation to refine the self-emission investigation.

Transmission difference between different tamper regions can also be investigated by post-processing the simulations. Since some fraction of heating radiation was absorbed by the FeMg foil, the tamper behind the foil may be less heated than the tamper on the tamper-only side. We want to investigate how the tamper conditions change with and without FeMg foil and how this transmission difference could affect the measured transmission and opacity.

Finally, the impacts of time- and space-gradient effects need to be investigated. Separate from the question of self-emission and tamper transmission difference, it is sensible to ask if the transmission measured over a 14% and 70% change in T_e and n_e can accurately represent the FeMg transmission at the inferred conditions (assuming the simulated gradient is correct). Since this is a synthetic investigation, we can turn off the complexity due to self-emission and tamper transmission difference and perform a simulated experiment to check how much disagreement we would expect solely due to the integration over the simulated temporal and spatial gradients. While departure from the LTE assumption is also a potential concern, it is beyond the scope of this paper and will be investigated elsewhere.

IV. NUMERICAL INVESTIGATIONS FOR POTENTIAL EXPERIMENTAL FLAWS

A. Simulation of SNL Z opacity experiments

SNL Z opacity experiments are simulated using a calibrated 1-D hydrodynamic model, which reproduces the measured plasma conditions and spectral image [8]. We used 1-D hydrodynamic simulations rather than 2-D/3-D simulations for practical purposes. The evolution of a tamped thin foil under volumetric heating is expected to be one-dimensional like, and the lateral uniformity is a reasonable approximation over the small sample subarea observed by the spectrometers. The negligible lateral gradient was confirmed experimentally[6]. Also, 1-D simulations are orders of magnitude faster than 2-D/3-D simulations and more practical for the systematic error investigations presented here.

First, the time-dependent spectral irradiance at the FeMg sample is estimated with the 3-D view-factor code VISRAD [9], using the measured 2-D ZPDH radiation time history and the measured in situ source-to-sample distances [17] as input. The target plasma evolution is then simulated with this heating spectral irradiance using the 1-D Lagrangian hydrodynamics code HELIOS [10, 11]. Finally, the image formation on the detector is simulated by solving radiation transport of the ZPDH radiation through the simulated sample and tamper plasma, accounting for the effects of the aperture and slits of the spectrometer.

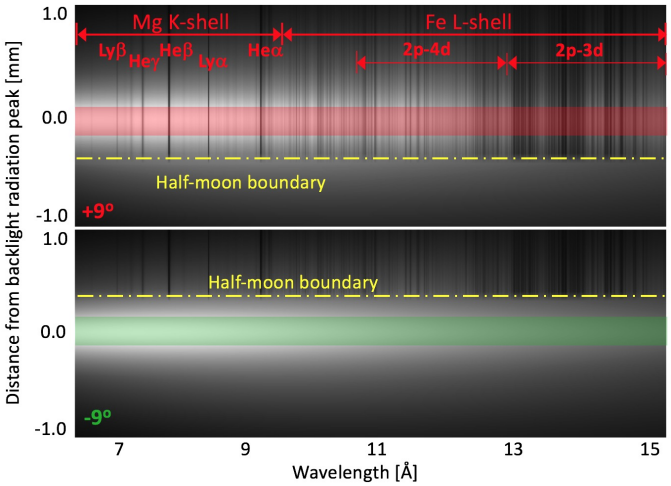

FIG. 3. (Color online) Simulated spectral image for +9°(top) and -9°(bottom) spectrometers. Due to the spatial resolution, finite source-to-sample distance, and ±9° line-of-sight difference, the backlight bright region appears on the FeMg-embedded side on +9° while it appears on the tamper-only side on -9°. Dark vertical lines are FeMg bound-bound absorption features.

T_e and n_e inferred from simulated spectra agreed with measured values for eight different experiments. The simulated backlighter spectral image also agrees with the measured spectral image both in spectral and spatial shapes and in brightness. These quantitative agreements support the soundness of the simulations [8]. In this section, we use these simulated experiments to assess the impact of plasma self-emission, tamper transmission difference, and time- and space-integration effects in the dynamic-gradient-plasma picture.

B. Analysis of simulated data: overall effects

We first simulate Z Fe opacity experiments for the *Thin CH* tamped target [see Fig. 1(a) for the target details]. These results provide an especially stringent test of simulation methodology since opacity models and measumrents agree in Ref. [4]. Figure 3 shows the spectral images simulated for spectrometers at ±9° for Fe and Mg areal densities of 6.4×10^{17} atoms/cm^2 and 7.5×10^{17} atoms/cm^2, respectively. The details of the simulation are discussed in Ref. [8]. The spectrometers provide spatial resolution along the aperture direction. Thus, the spectrometers at ±9° observe the backlight bright spot at different regions of the half-moon target as illustrated in Fig. 1(b). For the spectrometer at +9°, the

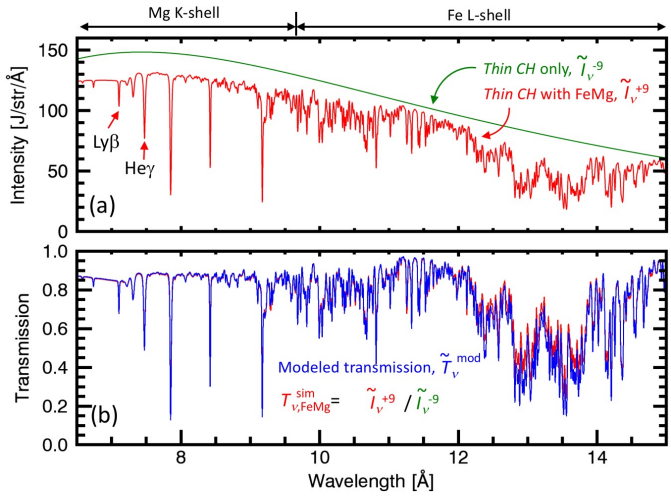

FIG. 4. (Color online) (a) Simulated spectra for the *Thin CH* tamper with the FeMg opacity sample (red) and the *Thin CH* tamper-only target (green). (b) Red curve is obtained by dividing the red curve in (a) by the green curve in (a). This is the imitation of our experimental data and takes into account i) self-emission, ii) tamper-transmission difference, and iii) axial- and temporal-gradient effects. The blue curve is the PrismSPECT FeMg transmission spectra computed at the single T_e and n_e value inferred from the Mg He-γ and Ly-β lines shown in (a). All spectra are convolved with instrumental broadening.

backlight radiation is centered on the FeMg-embedded side, and the FeMg b-b line absorption features clearly appear as dark vertical lines in the simulated spectral image in Fig. 3(top). There are Fe L-shell absorption lines (i.e., photon absorption by a transition of a bound electron in a state of principal quantum number $n = 2$ to higher excited states) above 9.5 Å and Mg K-shell lines (i.e., absorption by an electron in $n = 1$ to higher) below 9.5 Å, such as Mg Heα ($1s^2 \rightarrow 1s2p$), Heβ ($1s^2 \rightarrow 1s3p$), Heγ ($1s^2 \rightarrow 1s4p$), Lyα ($1s \rightarrow 2p$), and Lyβ ($1s \rightarrow 3p$). For the spectrometer at $-9°$, the backlight radiation is centered on the tamper-only side for the image at -9°, and the FeMg lines do not appear at the brightest region.

These spectral images take into account various effects that are neglected in the data analysis such as plasma self-emission over the entire duration, slight condition difference in the tamper on the FeMg-embedded side and tamper-only side, and the effect of the integration over the simulated spatial and temporal gradients. Thus, by analyzing such images in the same way as the measured spectra images in the static-uniform picture, we can test the validity of our data interpretation and check the importance of the neglected dynamic-gradient effects.

We first extract 300-μm spectral lineouts from the $\pm 9°$ spectral images by averaging over $\pm 150\,\mu$m centered at the brightest spot, which are indicated by the red and green horizontal bands, respectively. The extracted FeMg-attenuated and -unattenuated spectra are shown in Fig. 4(a) labeled as $\tilde{I}_\nu^{+9°}$ and $\tilde{I}_\nu^{-9°}$, respectively. The measured transmission spectrum is simulated by $T_{\nu,\,\mathrm{FeMg}}^{\mathrm{sim}} = \tilde{I}_\nu^{+9°}/\tilde{I}_\nu^{-9°}$. The effective T_e and n_e of the simulated FeMg plasma are inferred by analyzing the Mg He-γ and Ly-β in the same way as the data [6] and found to be to be 170 eV and $6.4 \times 10^{21}\,\mathrm{cm}^{-3}$. These values agree with the actual measurements within the measurement uncertainty [4, 6, 8]. The modeled transmission spectrum, $\tilde{T}_{\nu,\,\mathrm{FeMg}}^{\mathrm{mod}}$, is then computed at the inferred conditions taking into account the instrumental broadening as in Eq. (9). We call this a *point calculation* in this paper since it is calculated at a single T_e and n_e neglecting any sophisticated experimental issues.

Figure 4(b) compares the FeMg transmission spectrum from the simulated experiment $T_{\nu,\,\mathrm{FeMg}}^{\mathrm{sim}}$ (red) and the point calculation (blue). These FeMg transmission spectra are converted to the Fe opacity spectra by removing the Mg contribution[1], taking the natural log, and dividing them by the Fe areal density. The red and blue in Fig. 5(a) are opacity spectra with the dynamic-gradient picture and with the static-uniform picture, respectively. Their good agreement confirms negligible dynamic gradient effects. Thus, the simulation supports that the accuracy of the measured Fe opacity for the *Thin CH* case.

Similar comparisons are performed for the *CH+Be* [Fig. 5(b)] and *Thick CH* [Fig. 5(c)] cases. The effective T_e and n_e inferred from the simulated Mg spectra are $T_e = 194$ eV and $n_e = 3.8 \times 10^{22}\,\mathrm{cm}^{-3}$ and $T_e = 183$ eV and $n_e = 3.6 \times 10^{22}\,\mathrm{cm}^{-3}$, respectively, and agree with our experiments [4, 6, 8]. For *CH+Be* and *Thick CH* cases, the red and blue show large disagreement above 12.7 Å. This implies some of the dynamic-gradient effects are important in this range. This is the reason why we restricted the spectral range in Ref. [4] to below 12.7 Å. Compared to the *Thin CH* case, the disagreements for the *CH+Be* and *Thick CH* cases are slightly large even at wavelengths below 12.7 Å; however, the simulated effect (red) does not explain the measured higher-than-expected opacity (gray).

Nonetheless, the simulated dynamic-gradient effects are not completely negligible over the published range, especially for the *Thick CH* tamper case. The simulated opacity is $\sim$ 10–15% higher in the baseline and shows smaller peak-to-valley contrast in the b-b lines. Even though the discrepancies are roughly five times smaller than those reported in Ref. [4], they show a qualitatively similar trend. We scrutinize them further to identify the source of discrepancy in the following sections.

[1] The Mg contribution is removed by dividing the FeMg transmission spectra with the calculated Mg transmission spectra. The same technique is used in Ref. [4]. This approach removes the strong Mg b-b line featuers below 9.5 Å and Mg b-f continuum below 7.5 Å. Thus, the accuracy of the Fe b-f opacity below 7.5 Å is limited by the accuracy of the calculated Mg b-f opacity.

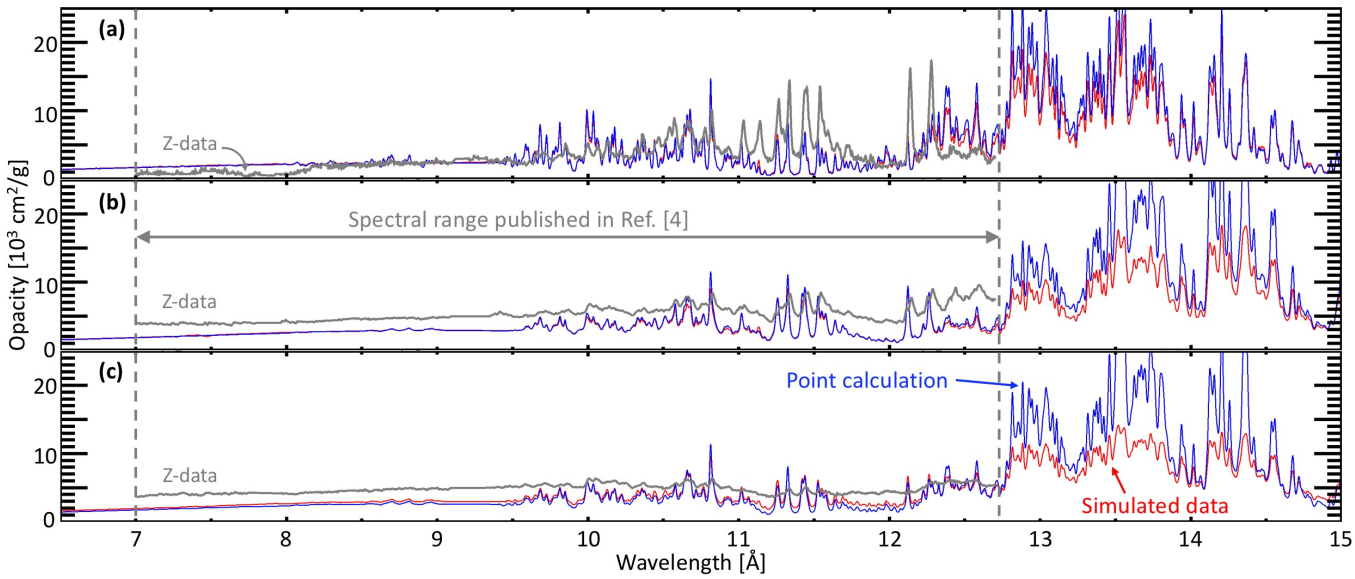

FIG. 5. (Color online) Comparison of the simulated (red) and modeled (blue) opacity spectra for the (a) *Thin CH*, (b) *CH+Be*, (c) and *Thick CH* cases. Instrumental broadening effects on the modeled spectra are taken into account in transmission spectra before converting them into opacity. Thick gray curves are the measured opacity from Ref. [4]. The discrepancies are not fully explained by any of the dynamic-gradient effects included in the simulation.

C. Impact of plasma self-emission

In 2009, Bailey *et al* [3] investigated the impact of 150-eV Fe-plasma self-emission by comparing it against ZPDH 314-eV blackbody radiation and concluded that self-emission contamination is negligible [see Fig. 15(a) of Ref. [3]]. However, this needs to be revisited for two reasons. First, our recent experiments reach considerably higher plasma temperature (∼195 eV) and the platform provides slightly higher brightness (∼350 eV). Since the increase in plasma temperature (30%) is higher than the increase in backlight radiation temperature (11%), the previous investigation may no longer be valid. Second, more importantly, the investigation discussed in Ref. [3] was done in a static-uniform picture and simply compared the self-emission and backlight spectral radiance, which is valid only when their solid angles, observable emitting areas, and durations are the same. Both the FeMg plasma and backlight source are 4 m away from the detector [Fig. 1(b)], and thus the difference in their solid angle to the detector is negligible. However, the area and duration can be quite different.

Figure 6(a) and (b) illustrate the +9° detector's view of the radiation source and the sample through the aperture. The red rectangle illustrates the area that a point on the detector would observe through the 50-μm slit. Each point on the detector records radiation integrated over this rectangle. The rectangle location depends on the position on the detector along the space-resolving direction (see Appendix of Ref. [8]). While the FeMg plasma has similar conditions across this red rectangle [6], the backlight radiation is not uniform within the rectangle and is bright over the full-width-at-half-maximum (∼0.6 mm) of its spatial distribution. This difference in radiation spatial variation has to be taken into account to accurately estimate the impact of the self-emission on the measurements.

Figure 6(c) shows time histories of the simulated self-emission and backlight radiation that the detector would observe through the aperture and the slit. While the backlight radiation peaks at stagnation, the plasma temperature peaks earlier when the sample heating-radiation-power peaks [Fig. 4 of Ref. [8]]. Figure 6(c) illustrates two important points. First, plasma temperature peaks earlier and reaches higher than 195 eV. Thus, while 195 eV inferred from the measured spectrum represents the temperature of the absorption features, it may not be a valid temperature for the self-emission investigation. Second, the plasma self-emission and backlight radiation time histories are very different and could have different durations. Furthermore, the tamper attenuation time history also has to be taken into account. Since the backlight and self-emission radiation peak at different times, the tamper attenuation may effectively block one more than the other depending on its time history. Thus, a simple spectral-radiance comparison can be inaccurate depending on these details.

The simulation discussed in Ref. [8] takes these details into account. The spectral image observed through the aperture and slit is simulated, accounting for the backlight radiation spatial variation, the FeMg+tamper plasma axial gradient, and their time histories. Thus, we can assess the impact of self-emission more accurately by extracting opacity from the simulated data computed with and without the self-emission.

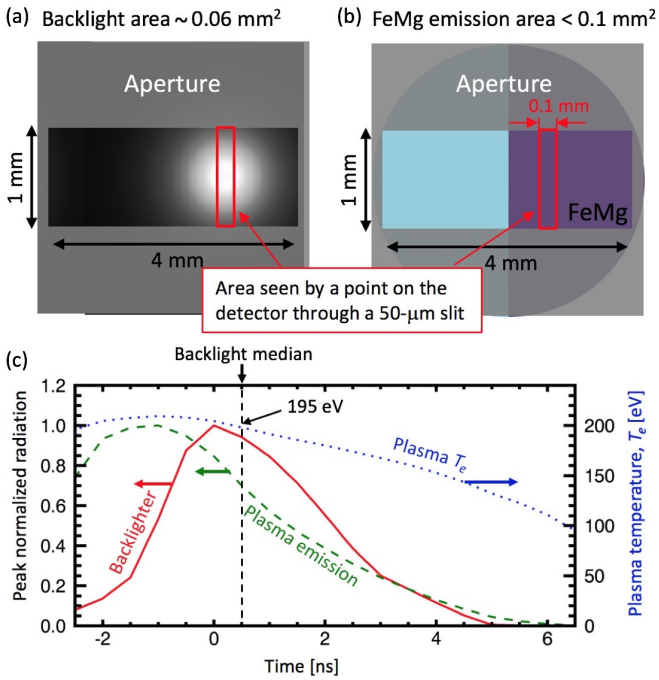

FIG. 6. (Color online) (a) Backlight radiation and (b) plasma self-emission observed by the detector through an aperture. The 50-μm slit further limits the detector view along the horizontal direction. The red rectangle illustrates the area that a point on the detector would observe through the aperture and slit. (c) Normalized time history of the simulated backlight radiation (solid red) and FeMg self-emission (dashed green). The FeMg self-emission peaks 1.5 ns earlier than the time of the backlight median. The FeMg temperature (dotted blue) peaks 8% higher than the inferred temperature which would produce 36% more emission than that of the the inferred temperature, 195 eV.

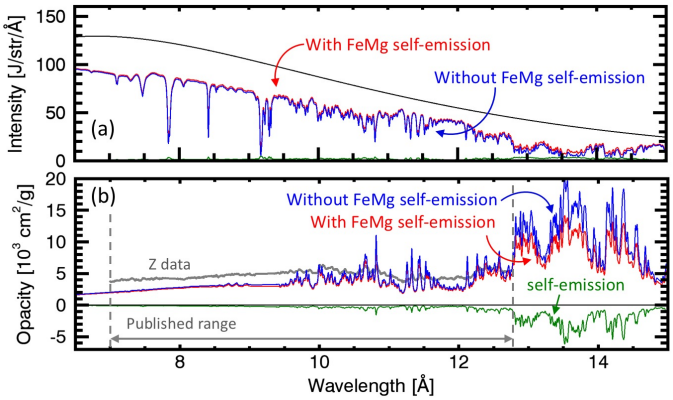

FIG. 7. (Color online) (a) Simulated FeMg-attenuated spectrum with (red) and without (blue) FeMg self-emission. The black curve (smooth curve on the top) is the backlight radiation without FeMg attenuation. The opacity spectra inferred from these simulations are shown in (b). The thick gray spectrum from 7 to 12.7 Å is the measured opacity published in Ref. [4]. The green curves at the bottom of each figure are red minus blue, indicating how much the self-emission would (a) increase the intensity spectra and (b) decrease the inferred opacity, respectively. The self-emission effect is always negative on the inferred opacity. The simulations rule out the hypothesis that discrepancies in the published range are produced by the self-emission.

Figure 7(a) shows the spectra simulated for the +9° spectrometer with (red) and without (blue) the FeMg self-emission using the *Thick CH* case as an example. This case was selected because the relatively high temperature renders self-emission more important than the other cases. The self-emission contribution is extracted by subtracting red by blue (green). This self-emission accounts for the sample axial gradient, signal attenuation in the tamper region, as well as the backlight radiation time history and the signal integration over the entire duration. The black curve is the FeMg-unattenuated spectrum simulated for the -9° spectrometer through the tamper-only side.

Figure 7(b) shows the opacity spectra inferred from these intensity spectra. They are inferred by dividing the red and blue by the black spectra in 7(a) to get transmission spectra and converted to opacity after removing the Mg contribution (see Sec. IV B for details). The green spectrum in Fig. 7 (b) shows the net self-emission effects computed by red (with) minus blue (without). The self-emission can be considered as negative opacity, and thus its effect always lowers the inferred opacity compared to the true value. This cannot be a correct explanation for higher b-f opacity in the measurement. This negative opacity can partially explain the smaller peak-to-valley contrast in the measured opacity, but the simulated peak-to-valley contrast is still significantly larger than the measured ones over the published range, $\lambda < 12.7$ Å. This verifies that the reported discrepancies were not caused by the FeMg self-emission effect.

Figure 8 compares the self-emission fraction defined as, $\epsilon_\nu / I_\nu^{\text{measured}}$. The green curve is computed by dividing the simulated self-emission (green) by the tamper-only-attenuated spectrum (black) of Fig. 7 (a). The red curve in Fig. 8 is simply computed by dividing 195-eV FeMg self-emission by the 350-eV Planckian backlight radiation in spectral radiance similar to Ref. [3]. We find that the self-emission investigation with this point calculation works reasonably well for our platform. At longer wavelength, both the point calculation and the simulation predict high self-emission but agree within a few percent. At shorter wavelengths, the point calculation underestimates self-emission fraction by a factor of two, but the fraction itself becomes smaller than 1% and does not impact our conclusion on the self-emission importance.

According to these simulations, the brighter plasma emission that occurs earlier than the backlight peak [i.e., green curve at $t < 0.5$ ns of Fig. 6(c)] does not contribute significantly for the *Thick CH* case. This is partly because the *Thick CH* tamper on top of the sample expands less, and its relatively low transmission partially blocks

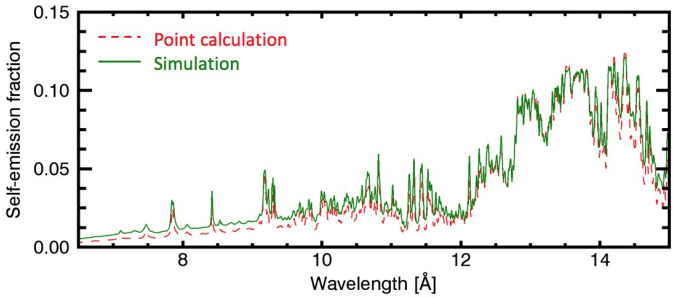

FIG. 8. (Color online) Self-emission fraction computed for point calculation (red) and detailed simulation (green). The red curve is a simple estimate based on 195-eV FeMg self-emission divided by 350-eV Planckian backlight radiation. The detailed investigation (green) taking into account duration and area differences verifies that the simple self-emission investigation (red) works reasonably well for our opacity platform.

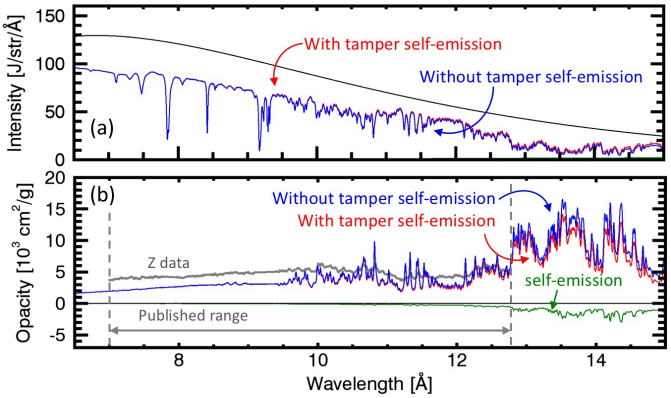

FIG. 9. (Color online) (a) Simulated data for the FeMg-unattenuated spectrum (black, top smooth curve) and the FeMg-attenuated spectra with (red) and without (blue) CH self-emission. The opacity spectra inferred from these simulations are shown in (b). The thick gray spectrum from 7 to 12.7 Å is the measured opacity published in Ref. [4]. The green curves on the bottom of each figure are red minus blue, indicating how much the self-emission would (a) increase the intensity spectra and (b) decrease the inferred opacity, respectively. The tamper self-emission effect is significantly smaller than FeMg self-emission and negligible over the published range.

the plasma self-emission early in time. While the simple self-emission investigation worked reasonably well for our platform, the impact of self-emission should generally be numerically or experimentally investigated in detail for every opacity platform, taking into account potential differences in duration, area, and solid angle. This is especially important for laser experiments when the backlight radiation is provided as a separate source and has a significantly shorter duration than the heating radiation (and thus shorter than the plasma self-emission). For such a platform, the self-emission estimated with the point-calculation neglecting the duration and area differences may significantly underestimate the true impact.

We repeat a similar investigation to assess the importance of the tamper self-emission. The results are summarized in Fig. 9. We find that tamper self-emission effect is even smaller than the FeMg self-emission[2].

D. Impact of tamper transmission difference

Tamper transmission can be slightly different on the FeMg-embedded and tamper-only sides due to extra absorption in FeMg region. Figure 10 (a) shows the T_e axial profiles simulated for the FeMg-embedded side (blue) and tamper-only side (red) for the *Thick CH* tamped target at the time of backlight peak. The spatial axis is given in log scale. The FeMg region (gray) is hotter than the tamper regions due to its higher opacity and its better energy coupling to the heating radiation. While the tamper regions have similar conditions on both sides, they are not identical. The thick top CH on the FeMg-embedded side has systematically lower T_e due to the reduced heating radiation caused by the extra attenuation in the FeMg region. As a result, the thick top tamper has notably lower transmission than those on the tamper-only side [Fig. 10(b)] and clearly violates the criterion, $T_a T_b = T_c$. Estimating the impact of this effect is not straightforward because the emergent spectra depend on the plasma axial gradients and the backlight radiation, which change over the experiment duration.

To quantify the impact of this tamper-transmission difference on the measured opacity, we simulate the *Thick CH* FeMg opacity experiment with and without enforcing $T_a T_b = T_c$. More specifically, the spectra transmitted through the tamper-only side are calculated in two different ways: i) using the tamper conditions simulated without FeMg ($T_a T_b \neq T_c$) and ii) using the tamper conditions simulated with FeMg embedded ($T_a T_b = T_c$). In the latter case, the attenuation in the tamper are forced to be identical and should cancel out at division, while the former takes into account the the imperfection of this cancelation. Figure 11(a) shows the resultant tamper-only spectra in red and blue, respectively. The black curve is the emergent spectrum attenuated by both the FeMg and tamper, $\tilde{I}_\nu^{+9^\circ}$. For each unattenuated spectrum (red and blue), the transmission spectra are computed then converted into opacity spectra [Fig. 11(b)]. The green curves are *with* minus *without* the tamper-transmission difference to quantify how much this effect would alter the measurement.

For the *Thick CH* case, the tamper transmission difference would artificially enhance the measured opac-

[2] Apparent "line" features in tamper self-emission are produced by the instrumental convolution and the non-linear transmission-to-opacity conversion and reflects the true impact on the measurement.

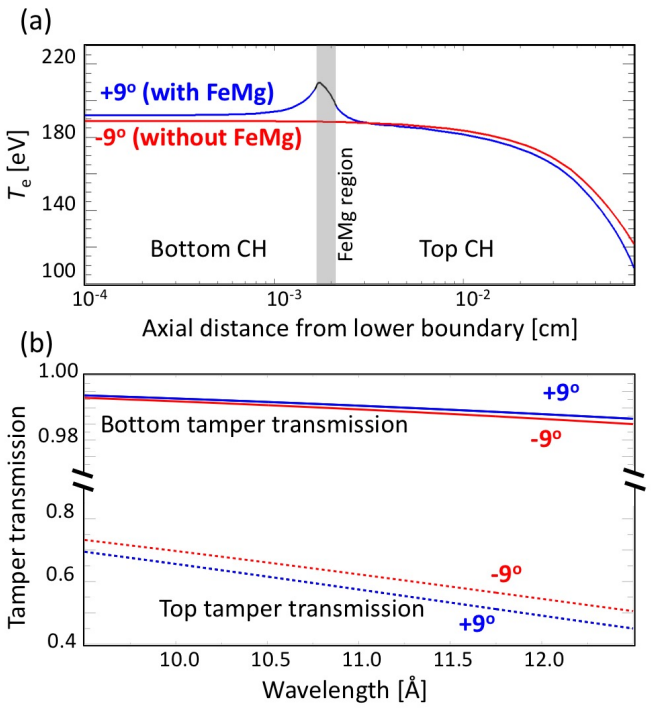

FIG. 10. (Color online) (a) $T_e(z)$ at the time of the backlight peak simulated for the *Thick CH* case with (blue) and without (red) FeMg sample. The shaded region indicates the FeMg region. (b) The resultant bottom tamper (solid) and top tamper (dotted) transmission spectra. While the bottom tamper transmission is slightly higher with FeMg, the top tamper transmission is significantly lower with FeMg due to extra attenuation of the heating radiation in the FeMg region.

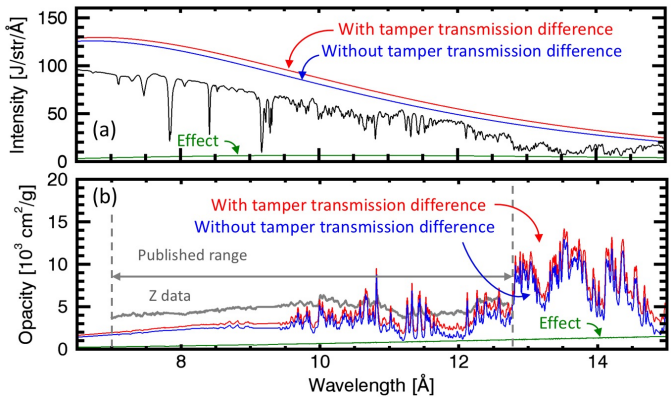

FIG. 11. (Color online) (a) Simulated spectra for the FeMg attenuated spectrum (black) and the FeMg unattenuated spectra with (red) and without (blue) the tamper condition difference. The opacity spectra inferred from these simulations are shown in (b). The green curves at the bottom of each figure show the simulated increase in measured opacity due to this effect. The thick gray spectrum from 7 to 12.7 Å is the data published in Ref. [4]. The effect is notable for *Thick CH* data, but it is too small to explain the observed discrepancy.

ity, and the error monotonically increases with wavelength. This artificial increase is 10–20% over the b-f region (λ = 6.5–10 Å). At longer wavelengths, this effect can artificially raise the opacity window at 12 and 14 Å by 40%. However, the simulated error is too small to explain the reported discrepancies. Besides, the measured opacity reported in Ref. [4] is corrected for this tamper-transmission-difference effect by subtracting the measured opacity by this simulated artificial opacity increase. Thus, the residual discrepancy reported in Ref. [4] implies either the observed discrepancy is real or the simulation underestimates its true impact.

The simulation also suggests that replacing CH by Be would remove this tamper-transmission-difference effect because the Be opacity is much lower than that of CH, and their transmission approaches unity, making their differences negligible (see Sec. IV F for details). However, in Ref. [4], we observed similar model-data discrepancies both with the *Thick CH* tamper and with the *CH+Be* tamper. This insensitivity to the choice of tamper material suggests that the observed b-f and window discrepancy are unlikely to be explained by the tamper-transmission difference.

E. Impact of temporal and axial gradient

In Ref. [8], our simulation found that the T_e and n_e decreased by 14% and 70%, respectively, over the backlight duration. This notable temporal gradient together with a subtle (<10%) axial gradient is a concern because we assume the measured opacity represents the Fe opacity at the inferred conditions. To isolate the impact of the temporal and spatial gradients, we numerically removed the other concerns that are the plasma self-emission (Sec. IV C) and tamper transmission difference (Sec. IV D). When the plasma self-emission and tamper transmission difference are turned off, the simulated spectra still account for the integration over the temporal and spatial gradients. Analysis of such spectra will answer i) if the integrated absorption features represent those at a single condition and ii) if the effective T_e and n_e inferred with a uniform Mg spectral model represent those of the Fe absorption features.

The solid and dashed curves in Fig. 12(a) are the simulated emergent spectra transmitted through FeMg+tamper and tamper-only, respectively. The FeMg and tamper self-emission is turned off. We used the same tamper transmissions to ensure $T_a T_b = T_c$ to remove the error associated with the tamper-transmission difference. The solid curve is divided by the dashed curve to get the simulated transmission, which is then converted to opacity after removing the Mg contribution. This simulated experimental opacity takes into account the effect of the spatial and temporal gradients in T_e, n_e, and backlight radiation [red, Fig. 12(b)]. The effective T_e and n_e are inferred from the simulated Mg spectra and found to be 194 eV and 3.8×10^{22} cm^{-3}, respectively, which are used

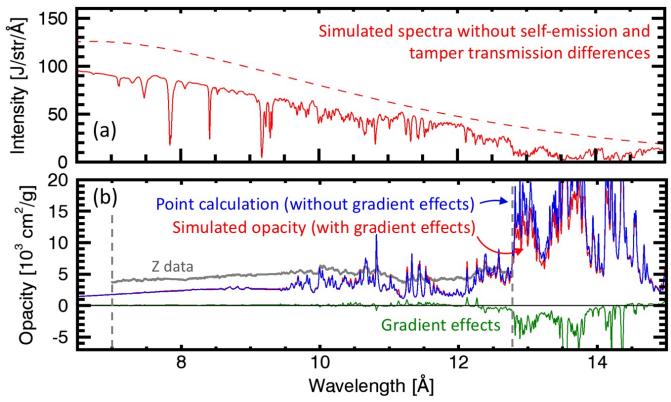

FIG. 12. (Color online) (a) Simulated attenuated spectrum without sample/tamper self-emission (solid) and unattenuated spectrum without tamper self-emission and tamper transmission differences (dashed). (b) The red curve is the inferred opacity spectrum from the simulation without the plasma self-emission and the tamper transmission difference. It is compared with the opacity spectrum calculated at the inferred conditions (i.e., $T_e = 195$ eV and $n_e = 3.8\times10^{22}\,cm^{-3}$). Instrumental broadening effects on the modeled opacity (blue) is applied on its transmission. The difference (green, the spectrum at the bottom) confirms that the integration over the predicted temporal and spatial gradients is negligible at $\lambda <$ 12.5 Å.

to compute the point-calculation opacity spectrum [blue, Fig. 12(b)].

The green curve is the simulated (red) minus modeled (blue) opacity spectra. Since we turned off the self-emission and error associated with the tamper-transmission difference, this difference picks out the impact of temporal and axial gradient on the measurements. In other words, the green curve represents the imperfection in the static-uniform-plasma picture employed in the data analysis. The gradient effect is negligible over the published range and becomes important at $\lambda > 12.7$ Å, which verifies that our analysis method does not introduce notable systematic uncertainty due to the static-uniform picture assumed in the data analysis.

F. Impact summary of each potential effect

In Sec. IV C- Sec. IV E, we reported the impact of the FeMg self-emission, tamper self-emission, tamper-transmission difference, and temporal and spatial gradient effects on the inferred opacity for the *Thick CH* case. Here, we repeat those investigations for the *Thin CH* and *CH+Be* cases and discuss the predicted impact on the measured opacity. Figure 13 summarizes the impact of (a) the FeMg self-emission, (b) the tamper self-emission, (c) the tamper-transmission difference, and (d) the temporal and spatial gradient effects, where the impact is defined as the simulated opacity with the effect minus that without the effect. We also show the gray curve that is the measured opacity minus a PrismSPECT[3] [18] opacity calculated at $T_e = 182$ eV and $n_e = 3\times10^{22}\,\mathrm{cm}^{-3}$ as an example to remind the level of disagreement reported in Ref. [4]. The gray curve showing positive values below 10 Å reflects the fact that the measured b-f and windows were higher than calculated. The gray curves showing downward spikes at b-b line locations reflects higher peak-to-valley contrast in the calculated b-b lines. If the reported discrepancy was caused by any of the issues investigated here, the green curve (i.e., $CH + Be$ case achieving $T_e = 182$ eV and $n_e = 3\times10^{22}\,\mathrm{cm}^{-3}$) would match the gray curve.

Figure 13(a) and (b) show the impact of FeMg and tamper self-emissions, respectively. This effect always lowers the inferred opacity and cannot be the correct explanation for higher measured opacity at the b-f and windows. This partially explains the difference in the peak-to-valley contrast [see the blowup of Fig. 13(a)], but the measured peak-to-valley contrast difference (gray) is four times larger and not fully explained by the simulated self-emission.

We also found slightly higher self-emission from the *CH+Be* case than the *Thick CH* case. We found this interesting because the inferred FeMg temperature was lower for the *CH+Be* case [Fig. 1(a)]. Based on the simulation, this happens because the early-time FeMg self-emission discussed in Sec. IV C is less effectively blocked by the optically thin CH+Be tamper. Furthermore, the predicted self-emission contamination above 12.7 Å is significant, and accurate opacity measurements above 12.7 Å may require accounting for the self-emission.

Figure 13(c) summarizes the impact of the tamper-transmission difference effect for each tamper configuration. As discussed in Sec. IV D, the tamper-transmission difference for the *Thick CH* case would increase the b-f and window opacity by 10–20% and 40%, respectively. The thick CH on the top of the sample was introduced to increase the sample T_e and n_e, which was initially suggested by simulations [19] and experimentally confirmed later [6]. To suppress this tamper-transmission effect without significantly lowering the T_e and n_e, we replaced the top thick CH with more optically thin Be (i.e., *CH+Be* shown in green). The impact of the tamper transmission difference increases as the tamper becomes opaque. For example, if we assume tamper opacity is different by 20% on the FeMg-embedded side and tamper-only side, it would produce the tamper-transmission-difference of only 1% when the expected tamper-transmission value is 0.95, while it would produce 13% when the expected transmission value is 0.5. The simulation result shown in Fig. 13(c) suggests that the tamper-transmission effect would be significantly sup-

[3] We use PrismSPECT for this model calculation. While the PrismSPECT calculation was not included in Ref. [4], it shows disagreement with the measured opacity very similar to those by the other models reported in this reference.

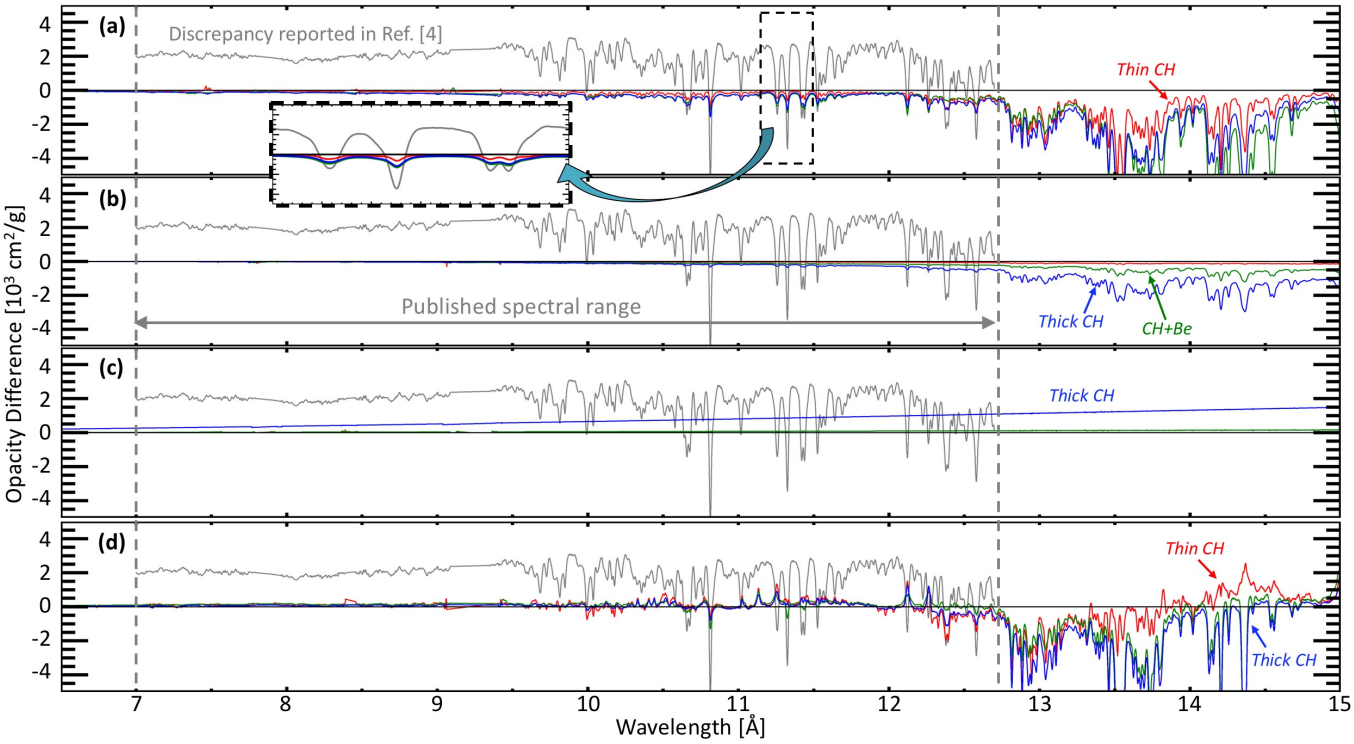

FIG. 13. (Color online) Summary of numerically assessed systematic errors on the opacity measurement associated with (a) FeMg sample plasma emission, (b) CH/Be tamper self-emission, (c) FeMg-embedded side and tamper-only side tamper transmission difference, and (d) time- and space-integration effects. The simulated inaccuracy is smaller (i.e., closer to zero) over the published range. The introduced systematic uncertainty is generally smaller for *Thin CH* (red) and larger for *Thick CH* (blue). The distinct gray curve shown from 7 to 12.7 Å is the discrepancy reported in Bailey *et al* [4]. None of the investigated effects explain the reported discrepancy.

pressed with *CH+Be* (green). The high transmission of the *CH+Be* tamper is also confirmed experimentally. Since we observe the higher b-f opacity even with the $CH + Be$ tamper, the tamper-transmission difference is not likely the correct explanation of the discrepancy.

Figure 13(d) summarizes the imperfection of the static-uniform assumption employed in the data analysis. The comparison confirms that the temporal and spatial gradient effects do not alter our conclusions at $\lambda < 12.7$ Å. The impact on the inferred opacity can be both positive and negative depending on the spectral range and reflects the complexity of the gradient effects in the experiments. The gradient effects become more important at longer wavelengths because i) the radiation at longer wavelength are contributed from lower-temperature radiation over longer duration, and ii) potential complexity due to transmission-opacity non-linear conversion at these low transmission (i.e., higher opacity) lines.

V. SUMMARY

We have performed a series of simulated experiments and investigated the impacts of the plasma self-emission, tamper transmission difference, and time- and space-gradient effects that were assumed to be negligible in the previous opacity analysis. The simulation reproduced the measured T_e and n_e and the spectral image of the backlight radiation [8], confirming it is appropriate for such quantitative numerical investigation. The overall effects were found to be too small to explain the discrepancies reported in Bailey *et al* [4].

The individual impact of each potential effect was investigated and reported. The self-emission effect was investigated taking into account the difference in area, duration, and solid angle between the self-emission and the backlight radiation. We found that the self-emission can slightly lower the line peaks. However, the effect was four times smaller than needed to explain the smaller peak-to-valley contrast observed in the experiments. The tamper-transmission difference effect on the *Thick CH* experiments is notable; it can systematically increase b-f and windows by 10–20% and 40%, respectively. However, the data shown in Ref. [4] were corrected for this based on the investigation reported here and therefore this does not account for the published model-data discrepancy. Also, the simulation suggests this effect should not be present in the data recorded with the *CH+Be* tamper. Since the opacity discrepancies in the b-f and window were observed from both tamper configurations,

the tamper-transmission difference is unlikely the source of discrepancy. While the simulation predicted a notable temporal gradient (i.e., 14% in T_e and 70% in n_e), the simulated experimental opacity closely represents the Fe opacity at the conditions inferred from the Mg spectra. Its impact on the opacity measurements and analysis was found to be too small to cause the severe discrepancies reported in Ref. [4].

There are limitations in the simulations such as the fixed dilution factor in the heating radiation, the lack of 2-D/3-D sample hydrodynamics, and a crude approximation of the upward pressure on the sample provided by the ZPDH plasma[8]. Future refined simulations without those limitations are desirable and could provide additional insight once they successfully reproduce the measured conditions and backlight spectral image.

ACKNOWLEDGEMENT

We thank the Z-facility teams for invaluable and dedicated technical assistance. We also thank S. B. Hansen for her expertise and useful discussion and R. E. Falcon for refining the manuscript.

Sandia National Laboratories is a multi-mission laboratory managed and operated by National Technology and Engineering Solutions of Sandia, LLC., a wholly owned subsidiary of Honeywell International, Inc., for the U.S. Department of Energy's National Nuclear Security Administration under contract DE-NA-0003525.

[1] S. Basu and H. M. Antia, Physics Reports **457**, 217 (2008).
[2] A. M. Serenelli, Astrophysics and Space Science **328**, 13 (2009).
[3] J. E. Bailey, G. A. Rochau, R. C. Mancini, C. A. Iglesias, J. J. MacFarlane, I. E. Golovkin, C. Blancard, P. Cosse, and G. Faussurier, Phys. Plasmas **16**, 058101 (2009).
[4] J. E. Bailey, T. Nagayama, G. P. Loisel, G. A. Rochau, C. Blancard, J. Colgan, P. Cosse, G. Faussurier, C. J. Fontes, F. Gilleron, I. Golovkin, S. B. Hansen, C. A. Iglesias, D. P. Kilcrease, J. J. MacFarlane, R. C. Mancini, S. N. Nahar, C. Orban, J. C. Pain, A. K. Pradhan, M. Sherrill, and B. G. Wilson, Nature **517**, 56 (2015).
[5] G. A. Rochau, J. E. Bailey, R. E. Falcon, G. P. Loisel, T. Nagayama, R. C. Mancini, I. Hall, D. E. Winget, M. H. Montgomery, and D. A. Liedahl, Phys. Plasmas **21**, 056308 (2014).
[6] T. Nagayama, J. E. Bailey, G. Loisel, S. B. Hansen, G. A. Rochau, R. C. Mancini, J. J. MacFarlane, and I. Golovkin, Phys. Plasmas **21**, 056502 (2014).
[7] S. Hansen, J. Bauche, C. Bauche-Arnoult, and M. F. Gu, High Energ. Dens. Phys. **3**, 109 (2007).
[8] T. Nagayama, J. E. Bailey, G. Loisel, G. A. Rochau, J. J. MacFarlane, and I. Golovkin, Phys. Rev. E **93**, 023202 (2016).
[9] J. J. MacFarlane, J. Quant. Spectrosc. Radiat. Transfer **81**, 287 (2003).
[10] J. J. MacFarlane, I. E. Golovkin, R. C. Mancini, L. A. Welser, J. E. Bailey, J. A. Koch, T. A. Mehlhorn, G. A. Rochau, P. Wang, and P. Woodruff, Phys. Rev. E **72**, 066403 (2005).
[11] J. J. MacFarlane, I. E. Golovkin, and P. R. Woodruff, J. Quant. Spectrosc. Radiat. Transfer **99**, 381 (2006).
[12] T. J. Nash, M. S. Derzon, G. A. Chandler, D. L. Fehl, R. J. Leeper, J. L. Porter, R. B. Spielman, C. Ruiz, G. Cooper, J. McGurn, M. Hurst, D. Jobe, J. Torres, J. Seaman, K. Struve, S. Lazier, T. Gilliland, L. A. Ruggles, W. A. Simpson, R. Adams, J. A. Seaman, D. Wenger, D. Nielsen, P. Riley, R. French, B. Stygar, T. Wagoner, T. W. L. Sanford, R. Mock, J. Asay, C. Hall, M. Knudson, J. Armijo, J. McKenney, R. Hawn, D. Schroen-Carey, D. Hebron, T. Cutler, S. Dropinski, C. Deeney, P. D. LePell, C. A. Coverdale, M. Douglas, M. Cuneo, D. Hanson, J. E. Bailey, P. Lake, A. Carlson, C. Wakefield, J. Mills, J. Slopek, T. Dinwoodie, and G. Idzorek, Rev. Sci. Instrum. **72**, 1167 (2001).
[13] J. E. Bailey, G. A. Rochau, R. C. Mancini, C. A. Iglesias, J. J. MacFarlane, I. E. Golovkin, J. C. Pain, F. Gilleron, C. Blancard, P. Cosse, G. Faussurier, G. A. Chandler, T. J. Nash, D. S. Nielsen, and P. W. Lake, Rev. Sci. Instrum. **79**, 113104 (2008).
[14] G. Loisel, J. E. Bailey, G. A. Rochau, G. S. Dunham, L. B. Nielsen-Weber, and C. R. Ball, Rev. Sci. Instrum. **83**, 10E133 (2012).
[15] J. E. Bailey, G. A. Rochau, C. A. Iglesias, J. J. Abdallah, J. J. MacFarlane, I. Golovkin, P. Wang, R. C. Mancini, P. W. Lake, T. C. Moore, M. Bump, O. Garcia, and S. Mazevet, Phys. Rev. Lett. **99**, 265002 (2007).
[16] T. Nagayama, J. E. Bailey, R. C. Mancini, C. A. Iglesias, S. B. Hansen, C. Blancard, H. K. Chung, J. Colgan, P. Cosse, G. Faussurier, R. Florido, C. J. Fontes, F. Gilleron, I. E. Golovkin, D. P. Kilcrease, G. Loisel, J. J. MacFarlane, J. C. Pain, G. A. Rochau, M. E. Sherrill, and R. W. Lee, High Energ. Dens. Phys. **20**, 17 (2016).
[17] T. Nagayama, J. E. Bailey, G. Loisel, G. A. Rochau, and R. E. Falcon, Rev. Sci. Instrum. **85**, 11D603 (2014).
[18] J. J. MacFarlane, I. E. Golovkin, P. R. Woodruff, D. R. Welch, B. V. Oliver, T. A. Mehlhorn, and R. B. Campbell, in *Inertial Fusion and Science Applications*, edited by B. A. Hammel, Amer. Nucl. Soc. (Proc. Inertial Fusion and . . . , 2004) p. 457.
[19] T. J. Nash, G. A. Rochau, and J. E. Bailey, Rev. Sci. Instrum. **81**, 10E518 (2010).